




Urea-assisted fabrication of $\text{Fe}_3\text{O}_4@\text{ZnO}@\text{Au}$ composites for the catalytic photodegradation of Rhodamine-B

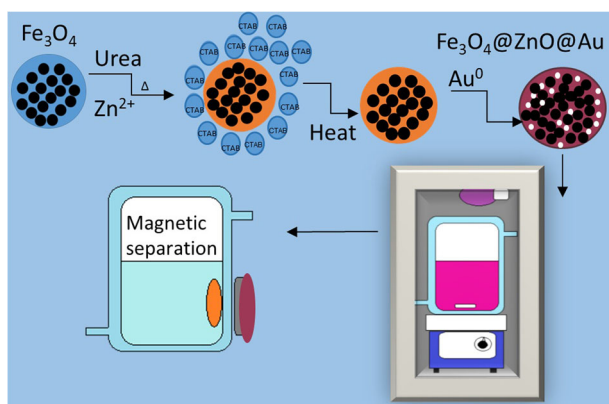
Robes Alves da Silva¹ · Marcos José Jacinto¹  · Virginia Claudia Silva¹ · Debora Cecília Cabana¹

Received: 7 November 2017 / Accepted: 10 February 2018
© Springer Science+Business Media, LLC, part of Springer Nature 2018

Abstract

A new chemical approach for the fabrication of Fe_3O_4 embedded ZnO magnetic semiconductor composite is reported. The method consists in increasing the pH of the synthesis solution by the thermal decomposition of urea instead of using common alkaline agents, such as NaOH and NH_4OH . The material ($\text{Fe}_3\text{O}_4@\text{ZnO}$) was used as a platform for the fabrication of highly dispersed gold nanoparticles (~5 nm). The catalytic efficiency of the material, $\text{Fe}_3\text{O}_4@\text{ZnO}@\text{Au}$, was tested in the photodegradation of Rhodamine-B solutions, and prominent catalytic efficiency, stability, and recycling were achieved. A single portion of the catalyst could be used up to five times without significant loss of activity and its photodegradation efficiency was considered high even after the 12th cycle (56%). Catalyst separation after each batch could be easily achieved because of the intrinsic magnetic property of the material. Leaching monitoring of free Zn species during the fabrication of the catalyst suggests that the use of urea decreased substantially the formation of non-magnetic-semiconducting species and provided a higher mass yield of the magnetic composite compared to an analogous protocol using NaOH. The catalyst was also characterized by detailed structural and chemical analyses, such as transmission electron microscopy (TEM), X-ray photoelectron spectroscopy (XPS), and vibration sample magnetometer (VSM).

Graphical Abstract



Keywords Magnetic composites · Photodegradation · Nanomaterials · Gold nanoparticles

✉ Marcos José Jacinto
marcjrd@pq.cnpq.br

¹ UFMT- Departamento de Química, Av. Fernando Corrêa da Costa,
Universidade Federal de Mato Grosso, 2367 - Boa Esperança,
Cuiabá, Mato Grosso 78060-900, Brazil

Highlights

- A novel mesoporous ZnO-modified magnetite as gold catalyst support has been synthesized.
- The amount of free Zn species in the solution was notably lower compared to traditional protocols.
- Enhanced photocatalytic performance was achieved towards the photodegradation of Rhodamine-B.
- The intrinsic magnetic property allowed an easy and straightforward catalyst separation.

1 Introduction

Semiconductors are considered a class of materials of great interest not mainly because of their conductivity but because their low band-gap energy (E_g) located in the 'visible' and 'near' ultraviolet spectral range ($\sim 1\text{--}3$ eV). Technological applications of this special class of materials include electronics, photonics and catalysis. Semiconductor assisted-photocatalysts have been extensively investigated for the decomposition of organic contaminants generated by industrial processes which pose a serious environmental threat [1] and [2]. Titania-based photocatalysts are largely the most common solids used to treat a various number of pollutants [3] and different TiO_2 nanostructures have been prepared, including nanowires, nanotubes, 3D hollow spheres and mesoporous materials [4]. Despite its photocatalytic efficiency and desiring chemical and optical stability a large scale water treatment system using TiO_2 as a photodegradation agent is still not economically feasible [4] and [5]. Therefore different alternatives have been proposed for the treatment of organic contaminants using other semiconducting materials. Among those semiconductor assisted photocatalysts, the use of Zinc oxide (ZnO) has been exhaustively studied mainly due to the fact that its bandgap energy (3.37 eV) is comparable to TiO_2 and It can taslo be applied in the photodegradation of organic compounds. Important features that put ZnO at the top of their class include electron mobility and lifetime, low cost production and the diversity of approaches available to the fabrication of different structures such as nanowires, nanoribbons, nanobelts, nanocombs, nanospheres and nanofibers [6]. A photodegradation using a semiconductor requires an absorption of a photon of energy equivalent to E_g (band gap energy). The photon migration leaves a vacancy (hole) behind in the valence band and the organic mineralization is promoted by the hydroxyl and superoxide radicals generated by the reaction of H_2O with a hole, and the combination of free electrons and molecular O_2 [7]. A recombination of holes/free electrons prior to the formation of the radical species is a limiting factor for the photodegradation efficiency and must be prevented. One suitable way to accomplish that is achieved by doping the semiconductor material with another semiconductor or metal nanoparticles. The presence of a dopant increases charge separation (free electrons/holes) and minimizes electron-hole combination [8]. A great variety of methods which include precipitation, sol-gel route, hydrothermal synthesis, and electrochemical deposition processes

have been reported for the fabrication of ZnO, and It is a well-known fact that the solid morphology is a hotspot for the catalyst efficiency towards the mineralization of an organic target [9]. Representative ZnO-mesoporous structures are of great interest because of their large surface area, void pore volume and tunable porosity [10] and [11]. In supported liquid-phase catalysis, the large pores of such material permit better diffusion of the molecule throughout the solid matrix which renders a higher catalytic activity [12]. One important step after the photodegradation of a targeted organic contaminant is the separation of the catalyst from the effluent stream. The separation is not only important for the final purification of the treated effluent but It is also indispensable for catalyst recycling. Magnetic separation constitutes a simple and straightforward method that has recently been used as a new approach for catalyst separation [13]. Nguyen et al. synthesized a magnetic compound combining Fe_3O_4 with ZnO and applied it in the photodegradation of textile dye. Under the established conditions a single portion of the catalyst could be magnetically recycled up to three times [14]. A key point for the successful fabrication of a biphasic (magnetic/catalytic) composite is to achieve selectivity towards the formation of the catalyst phase around the magnetic component. This step is critical for catalyst stability and for lessening the leaching of non-magnetic catalytic species in liquid phase after the photoreaction is carried out. In this study, a new magnetic composite ($\text{Fe}_3\text{O}_4@\text{ZnO}@\text{Au}$) was obtained and applied as a reusable catalyst for the photodegradation of Rhodamine-B. The mesoporous ZnO layer was obtained controlling the pH elevation by the decomposition of urea. The Zn concentration was monitored during the catalyst fabrication and it was observed that the leaching of Zn into the liquid media, after the magnetic separation of the new solid, was considerably inferior to that obtained after the fabrication of an analogous material using NaOH as the pH modifier. The composite was applied in the photodegradation of Rhodamine-B solutions and remarkable properties concerning the catalyst efficiency and recycling were obtained.

2 Experimental methods

2.1 Synthesis of mesoporous $\text{Fe}_3\text{O}_4@\text{ZnO}$

The magnetic nanoparticles (~ 12 nm) were obtained according to the method previously reported by [15] with

some slight modifications. Briefly 3,90 mmols of iron oleate (freshly prepared) were added to a three-neck round-bottom flask containing 75.8 mmols of octadecene and 19.3 mmols of oleic acid. The solution was heated to up to 315 °C (~ 5.5 °C min^{-1}) and kept at this temperature for 10 min. The magnetic fluid was then cooled to room temperature and centrifuged to remove large aggregates. Freshly prepared Fe_3O_4 nanoparticles were then coated with a ZnO layer. For this purpose, the magnetic fluid was dispersed under vigorous mechanical stirring in a solution of ethanol and ethyl acetate ($1V_{\text{et}}/2V_{\text{eac}}$), the Fe_3O_4 nanoparticles were magnetically collected using a small magnet (4000 G). In order to obtain water dispersed Fe_3O_4 nanoparticles, 20 mL of a 137 mmol aqueous solution of cetyltrimethylammonium bromide (CTAB) were added to the Fe_3O_4 nanoparticles and the mixture was magnetically stirred for 30 min (4000 rpm) to promote the surface replacement of oleic acid by CTAB. The mixture was then added to another three-neck round-bottom flask containing 250 mL of a Zn (CH_3COO)₂ (0.46 M)/Urea (0.40 M) solution and kept under magnetic stirring for 8 h at 85 °C. The material [$\text{Fe}_3\text{O}_4\text{-Zn(OH)}_2$] was then collected magnetically and washed twice with distilled water. Finally $\text{Fe}_3\text{O}_4\text{-ZnO}$ composite was obtained by calcining the material at 300 °C for 3 h. For comparison purposes, $\text{Fe}_3\text{O}_4\text{-ZnO}$ was also obtained using a NaOH solution as the source of OH^- for the precipitation of Zn(OH)_2 . The synthetic protocol used in this step was the same except that a NaOH solution (0.01 M) was used in substitution of Urea to reach the desirable pH (12).

2.2 Obtention of $\text{Fe}_3\text{O}_4\text{@ZnO@Au}$

To enhance the catalytic properties of the magnetic semiconductor catalyst, the material was doped with Au nanoparticles. For this purpose, 150 mg of $\text{Fe}_3\text{O}_4\text{@ZnO}$ was added to 50 mL of an aqueous solution containing 7.7 mg of HAuCl_4 and 1.0 g of urea. The mixture was kept under magnetic stirring for 2 h at 70 °C, and then 5 mL of an ethanol solution of NaBH_4 (~ 2.0 mg) was added. The solution was stirred for 3 h and the material ($\text{Fe}_3\text{O}_4\text{@ZnO@Au}$) was finally magnetically collected, washed three times with distilled water and calcined at 350 °C (1 h).

2.3 Photocatalytic tests

The photocatalytic activity of $\text{Fe}_3\text{O}_4\text{@ZnO@Au}$ towards the degradation of Rhodamine-B was investigated under visible light using a high-pressure mercury-vapor lamp (400 W). In a typical experiment, 100 mg of the catalyst was added to 50 mL of an aqueous solution of Rhodamine-B (25 ppm) placed in a double-jacketed water-cooled glass vessel connected to a circulating bath (15 °C). A double-

glass (SiO_2) jacket was used as a UV cut-off filter. Prior any light exposure the mixture was magnetically stirred in the dark for 30 min to reach the adsorption equilibrium. In the next step, the lamp was switched on and the photoreaction was carried out according to the established reaction time (up to 8 h). After the reaction time was complete, the catalyst was magnetically collected by placing a small Nd magnet (4000 G) on the reactor wall, and the photo-degraded liquid sample was taken out for quantitative analysis which was carried out using a spectrophotometer UV-vis.

2.4 Instruments

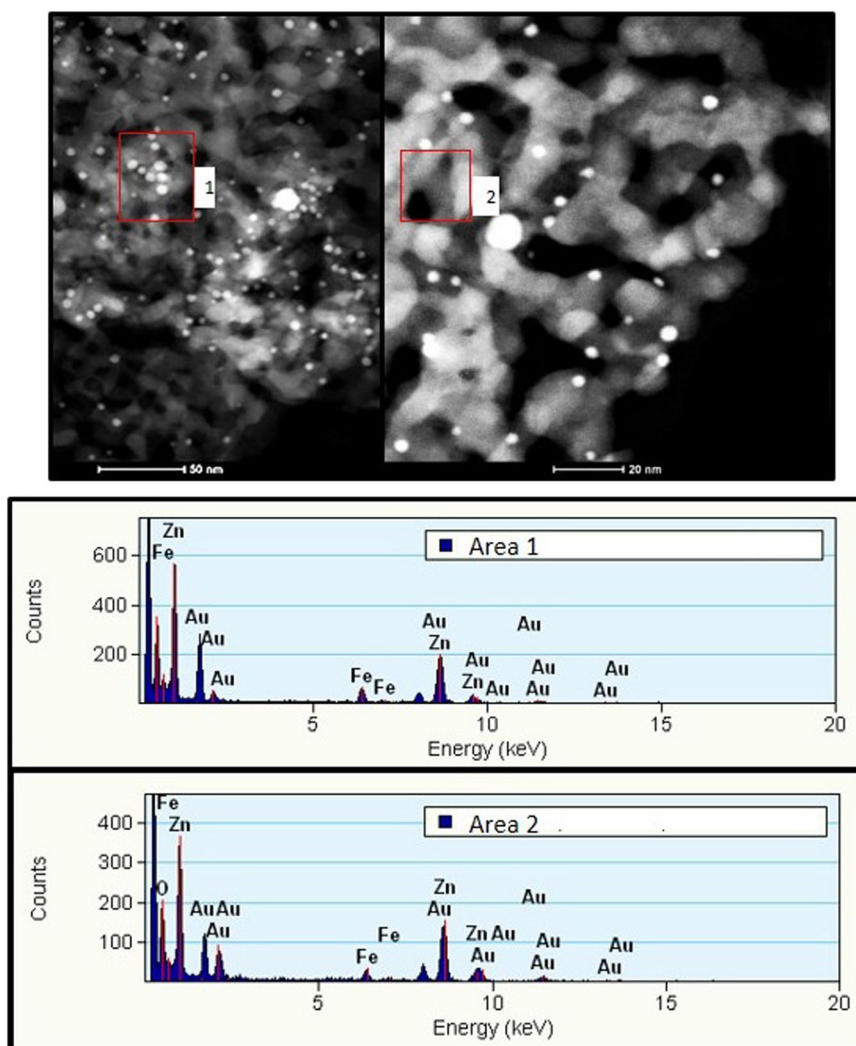
For a detailed characterization profile the catalysts were morphologically characterized by several techniques. XPS analysis was performed on a K-alpha XPS (ThermoFischer Scientific, UK) using Al $K\alpha$ X-rays (vacuum $>10^{-8}$ mbar). High resolution spectra were obtained using a pass energy of 0.1 eV. The peak C1s at 284 eV was used as the binding energy reference. X-ray diffractions patterns (XRD) were collected on a Siemens D5005 with Cu $K\alpha$ radiation at 40 kV. TEM was carried out on a FEI TECNAI F20 HRTEM operating at 200 kV. The specimens were prepared by suspending the sample in ethanol and water ultrasonically and placing a drop of the mixture onto a copper grid with amorphous carbon film (200 mesh). Elemental compositions and elemental mapping of the materials were obtained by an energy-dispersive spectrometer (EDS) connected to the electron microscope. Surface areas, diameter and pore volume were determined from N_2 adsorption experiments in a Quanta-chrome NOVA 2200 analyzer. UV-vis experiments were performed in a Femto-Cirrus 80 MB UV spectrophotometer using quartz cuvette (10 mm path length). Metal concentration profile in the catalysts was measured by X-ray fluorescence spectrometer and ICP-AES using a Spectro Arcos analyzer.

3 Results and discussion

3.1 Catalyst characterization

The magnetic nanoparticles were coated with a mesoporous layer of ZnO by the thermal decomposition of urea under heat. The method allows a slow rise in pH which leads to the precipitation of $\text{Zn(OH)}_2/\text{ZnO}$. It was found that the use of urea instead of other alkaline agent such as NaOH favors the formation of zinc hydroxide layer on the surface of the magnetic particles. In a typical synthesis protocol, the concentration of Zn species in the solution after the solid was isolated magnetically was 22.4%, as determined by ICP-AES. The concentration increased to 66.7% when

Fig. 1 STEM images (1 and 2) of $\text{Fe}_3\text{O}_4@\text{ZnO}@\text{Au}$ composite. EDS analysis of selected regions contained in box 1 and 2 (insets of 1 and 2)



NaOH solution was used for the formation of ZnO. Since the quantity of reactants, final volume solution, temperature and the stirring magnetic speed were the same for both protocols the superior lower leaching of Zn species, obtained using the decomposition of urea as the alkaline agent, strongly suggests that its use promotes a higher selectivity to the formation of ZnO around the magnetite nanoparticles. Thus, the concentration of free diamagnetic ZnO particles in the solution after the magnetic isolation is lower (22.4 %). The superior higher leaching of Zn using NaOH led to a significant decrease in the synthesis efficiency and the route using urea provided a higher mass yield than the analogous protocol using NaOH. In a typical experiment the final composite mass obtained using urea was $\sim 1.5\times$ higher (final mass 137.5 mg) compared to the route using NaOH (92.0 mg). These results are doubly important because the use of urea as the alkaline agent not only constitutes a cleaner method compared to NaOH but it also increases the atom economy and reaction mass efficiency which are considered important parameters in the

search for green synthetic routes. Kandula and Jeevanandam [16] fabricated core-shell $\text{SiO}_2@\text{Co}(\text{OH})_2$ by the thermal decomposition of urea and proposed that the silica coating mechanism occurs by an adsorption–nucleation–coalescence–anisotropic growth–self-assembly pathway where the presence of urea induced the Co^{2+} adsorption on the silica surface as a complex, $\text{Co}(\text{NH}_3)_y$. We believe that a similar migration of Zn^{2+} ion to the magnetite surface occurs forming a $\text{Zn}(\text{NH}_3)_y$ complex. Urea then undergoes hydrolysis and produces $\text{Zn}(\text{OH})_2$ which can then be transferred to the Fe_3O_4 through an ion-exchange process facilitated by the presence of CTAB. An important step during the precipitation of the $\text{Zn}(\text{OH})_2$ is the control of pH since the excess of OH^- ion in the solution leads to the formation of $\text{Zn}(\text{OH})_4^{2-}$ which is highly soluble in water. Therefore, fabrication of $\text{Zn}(\text{OH})_2$ using common alkaline agents must be carried out under a rigorous control of pH. In this novel methodology, the use of urea even in high amounts (6 g) does not cause a significant release of OH^- in solution (pH ~ 9). Thus, no pH monitoring during the

Fig. 2 X-ray mapping of a selected area for O, Fe, Zn and Au

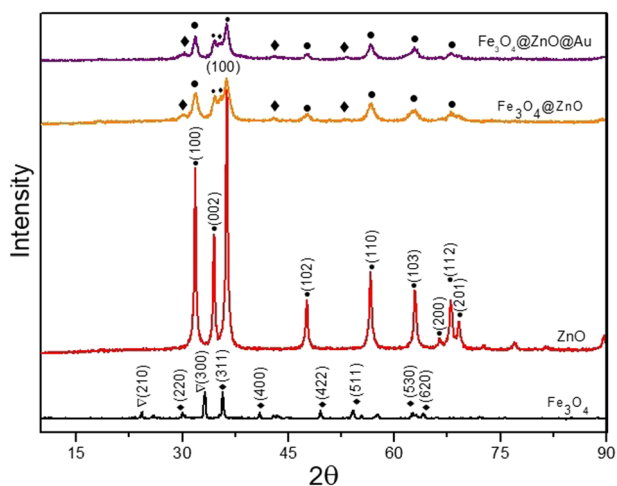
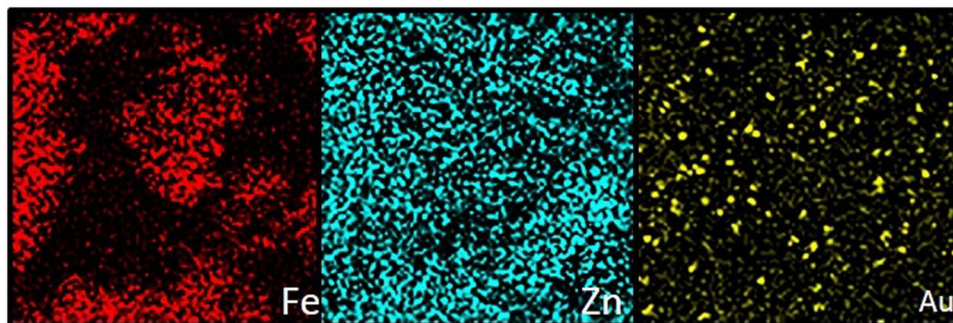
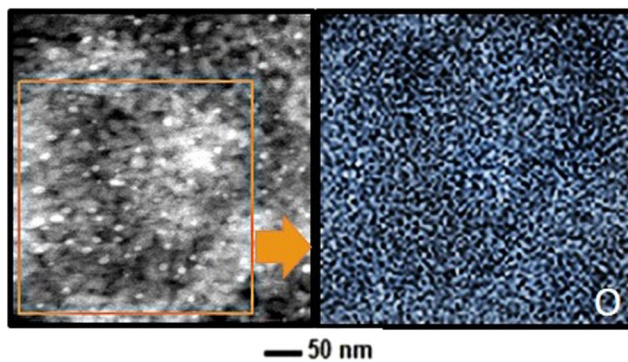


Fig. 3 XRD patterns of the as-prepared $\text{Fe}_3\text{O}_4@ZnO@Au$ by the thermal decomposition of urea

reaction is required which greatly simplifies the work-up procedure.

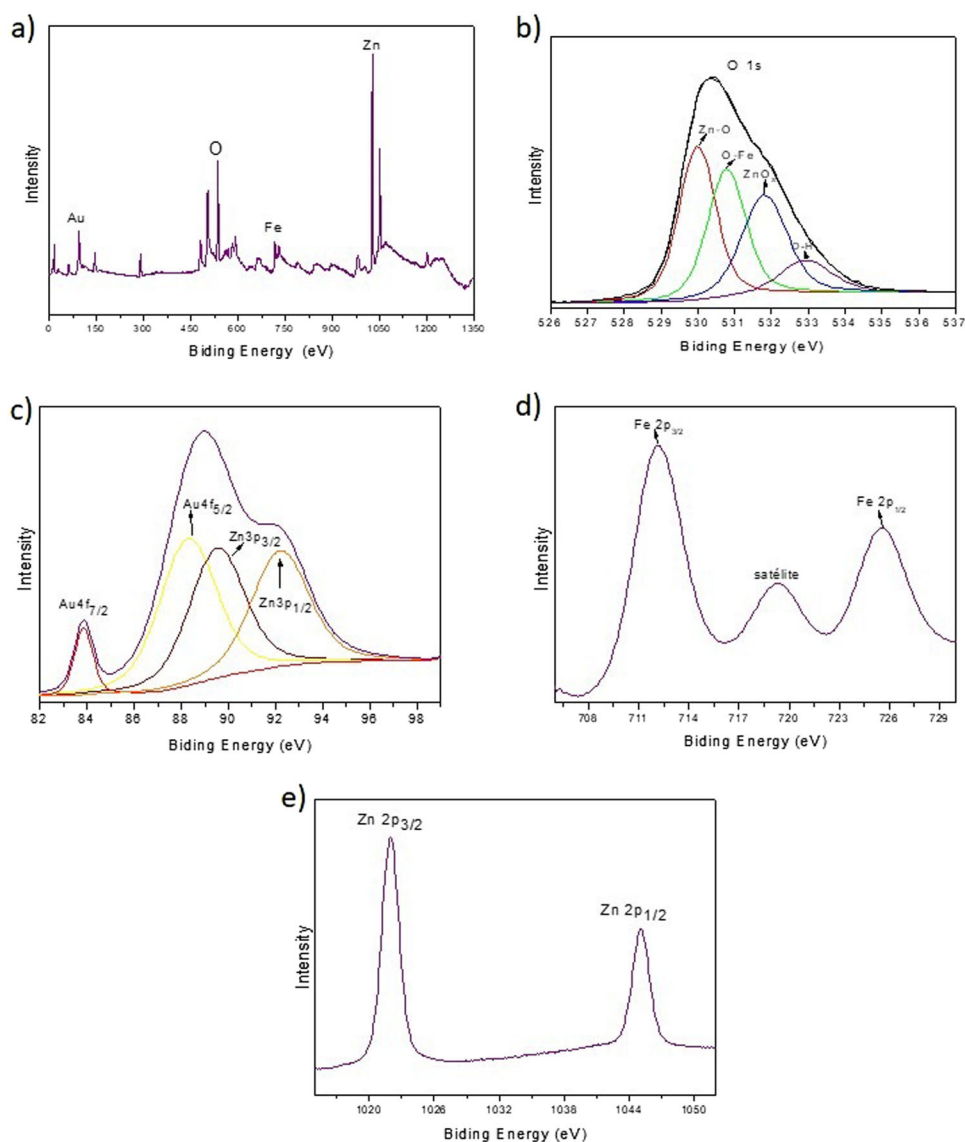
Figure 1 shows the TEM images for the composite $\text{Fe}_3\text{O}_4@ZnO@Au$ obtained using the thermo decomposition of urea calcined at 350 °C. The ZnO film exhibits the form of interlocking nanoworm structures giving rise to a mesoporous matrix (porous size ~11.7 nm) which is available as a template for “in situ” generation and trapping of Au nanoparticles. The estimated porous size obtained from the TEM image is in good agreement with the pore size obtained using the Barrett–Joyner–Halenda method (12 nm) and confirms the mesoporous character of the ZnO matrix. EDS analysis of two distinct areas (inset of Fig. 1) shows, as

expected, the presence of Zn, Fe and Au. The bright well-dispersed white spots (~5 nm) are attributed to the presence of gold nanoparticles which are also confirmed by EDS.

The Au metal nanoparticles have electron density significantly higher than Zn and Fe and are clearly identified in the TEM image. However It is not possible to distinguish the magnetic phase (Fe_3O_4) from the semiconducting phase (ZnO) because of their similar electron density distribution. In order to obtain a detailed size-distribution and composition-distribution of the catalyst and a better distinguishing of the magnetic and the semiconducting phases, a complete elemental mapping analysis was also obtained by energy dispersive x-ray. It can be seen from Fig. 2 that the as-obtained $\text{Fe}_3\text{O}_4@ZnO@Au$ is constituted of a core-shell structure containing individual Fe_3O_4 nanoparticles enwrapped by a ZnO mesoporous structure containing Au metal nanoparticles. It is also clear from the Fe mapping that the magnetic nanoparticles are approximately spherical in shape. Au mapping confirms that the white spots previous observed in Fig. 1 are indeed highly dispersed gold nanoparticles (~5 nm) attached to the ZnO mesoporous structures.

The diffraction patterns (XRD) of the composite $\text{Fe}_3\text{O}_4@ZnO@Au$ are displayed in Fig. 3. The results show that the crystallinity of both ZnO and Fe_3O_4 is maintained after the enwrapping of the magnetic particles by the semiconducting phase followed by its calcination and the deposition of Au nanoparticles. The main peaks at 2θ values of 31.94°, 34.40°, 36.16°, 47.41°, 56.55°, 62.88°, 66.39°, 68.15° e 69.20° correspond to the (100), (002), (101), (102),

Fig. 4 XPS spectra of the $\text{Fe}_3\text{O}_4@\text{ZnO}@\text{Au}$ composite **a** Survey spectrum. **b–e** XPS spectra of O, Au, Fe and Zn core levels, respectively



(110), (103), (200), (112) and (201) planes characteristic of hexagonal ZnO wurtzite [17]. For the magnetic matrix, peaks at 2θ values of 29.48° , 36.00° , 42.25° , 52.29° , 57.73° , 67.65° and 69.56° are found which can be attributed to the (220), (311), (400), (422), (511), (530), (620) Fe_3O_4 planes [18] and [19]. The peaks at 2θ : 22.69° e 33.01° correspond to the (210) and (300) maghemite planes ($\gamma\text{-Fe}_2\text{O}_3$) which were probably obtained due to the oxidation of Fe^{2+} during the calcination step [20]. The presence of Au cannot be clearly identified by XRD probably because of its low concentration (4.67%, as determined by XRF) and its reduced size, which can lead to a decrease in the crystallinity of the material.

XPS was used to analyze the surface chemical composition of the material and to elucidate the chemical state of the gold species. The survey spectrum (Fig. 4a) shows distinctive peaks corresponding to Zn, Au, Fe and O. The

presence of such species is in good agreement with the composite composition. The high resolution spectrum of Zn_{2p} (Fig. 4e) shows two peaks at 1021.8 eV and 1045.2 eV, which are attributed to $\text{Zn}2p_{3/2}$ and $\text{Zn}2p_{1/2}$. In this work, the difference on the binding energy for the two $\text{Zn}2p$ peaks for the bare semiconductor-magnetic-composite ($\text{Fe}_3\text{O}_4@\text{ZnO}$) is 22.8 eV. The shift in energy difference to a larger value (0.5 eV) obtained for the material after the deposition of the Au nanoparticles is most likely to be associated with Au/ZnO interactions such as electron transferring from the semiconductor (ZnO) to the Au particle surface [21]. The difference in binding energy between the Zn peaks and presence of an O1s peak at 530.6 eV clearly suggest the formation of ZnO [1]. High resolution XPS spectrum of Au 4f (Fig. 4c) shows two components at 83.7 and 88.4 eV corresponding to Au $4f_{7/2}$ and $4f_{5/2}$ and confirms the presence of metal gold. The

negative shift of 0.3 eV in comparison to 84.0 eV of bulk Au is another evidence for the strong interaction between the semiconducting phase and the Au NPs possibly caused by electron transfer phenomenon [22]. The XPS spectra for the Fe 2p (Fig. 4d) level is split into Fe 2p_{3/2} and Fe 2p_{1/2} components with spin-orbit-splitting at 726.5 and 712.0 eV, respectively. These peaks are attributed to the presence of Fe²⁺ with Fe³⁺ and confirm the successful fabrication of Fe₃O₄. The satellite peak at 719.3 eV suggests the partial oxidation of Fe₃O₄ to γ -Fe₂O₃ which probably occurred during the calcination step [23] and [24].

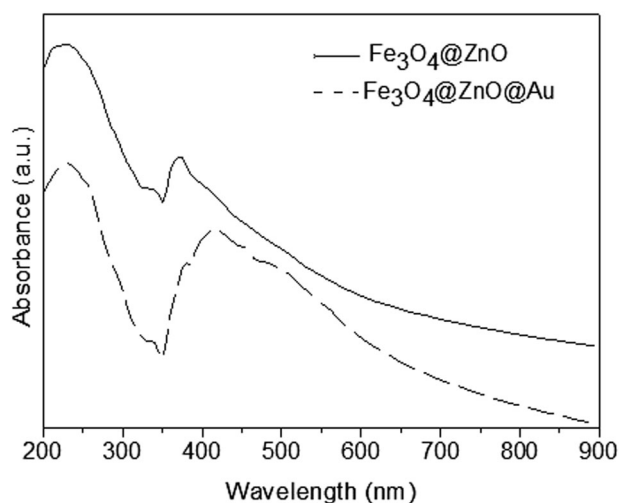
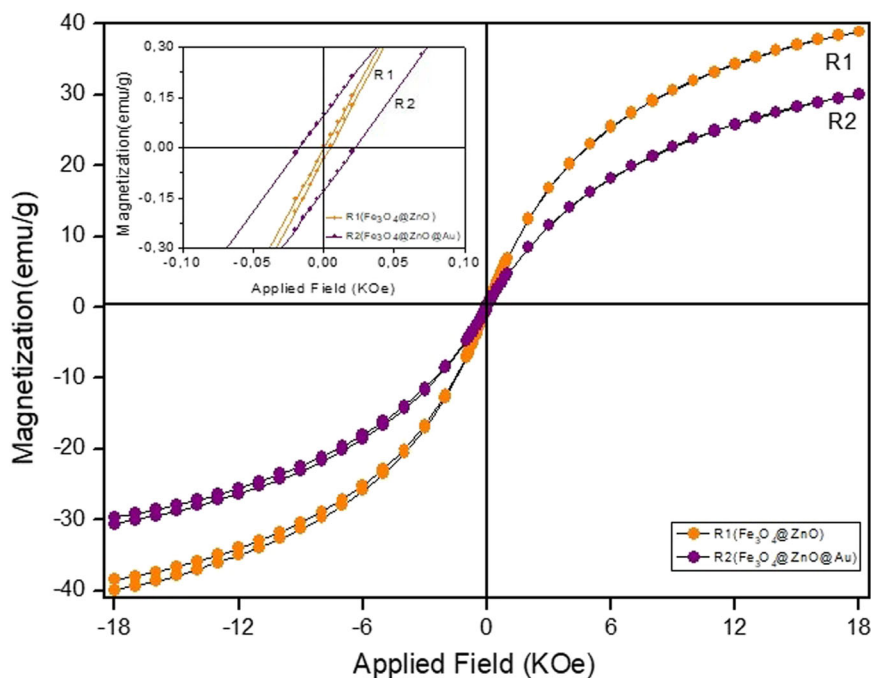


Fig. 5 UV-vis spectra for Fe₃O₄@ZnO@Au and Fe₃O₄@ZnO obtained by measuring the absorption of powder samples dispersed in water

Figure 5 exhibits the molecular absorption spectroscopy of the Fe₃O₄@ZnO@Au and Fe₃O₄@ZnO composites in the UV-vis range. The band at 372 nm found for Fe₃O₄@ZnO is consistent with the formation of ZnO particles. This band is also present in the Fe₃O₄@ZnO@Au spectrum in a lower frequency (379 nm). This shift in energy can be explained in terms of the Au electronegativity which induce metal gold nanoparticles to withdraw electron density more towards itself [25]. Another band centered around 530 nm is observed for the Fe₃O₄@ZnO@Au spectrum which is characteristic of surface plasmon absorption of small Au nanoparticles [1]. The decrease in absorbance intensity of ZnO band for Fe₃O₄@ZnO@Au is probably due to the presence of Au nanoparticles and It suggests that the material is more photoactive in the UV-vis range [26].

To investigate the magnetic properties of the catalysts the room-temperature hysteresis loop of the materials was measured using VSM. The magnetic behavior are shown in Fig. 6 and suggest that both materials (Fe₃O₄@ZnO@Au and Fe₃O₄@ZnO) present superparamagnetic properties since no hysteresis and coercivity is appreciably observed for the magnetic hysteresis loop. The saturation magnetization for both catalysts is considerably lower than that observed for pure magnetite (~80 emu g⁻¹) which can be explained in terms of the presence of diamagnetic species (ZnO and Au). Despite the lower magnetization the materials can still be quickly collected from aqueous solutions by applying a magnetic field using a small magnet (4000 G). The superparamagnetic property of the material enables it to be quickly dispersed in solutions once the

Fig. 6 Hysteresis loops for the Fe₃O₄@ZnO@Au and Fe₃O₄@ZnO materials



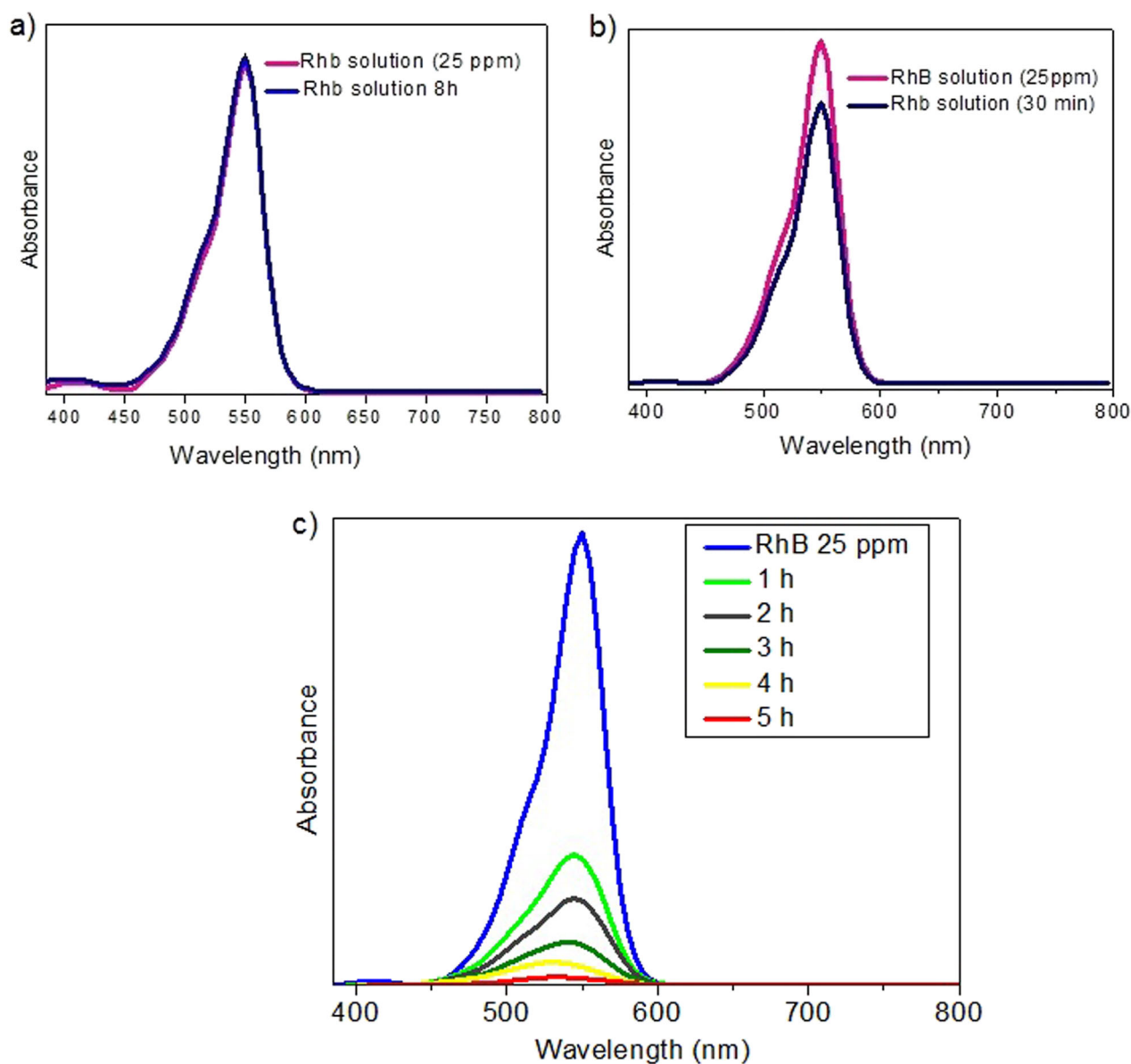


Fig. 7 UV-vis spectra of **a** catalyst absorption experiment in the dark **b** photolysis study in the absence of catalyst **c** degradation of Rhodamine-B photo-catalyzed by $\text{Fe}_3\text{O}_4@\text{ZnO}@\text{Au}$. Conditions:

100 mg of catalyst (**a** and **c**), 50 mL of an aqueous solution of Rhodamine-B 25 ppm, Temperature = 15 °C

magnetic field is removed. From a perspective of a potential catalytic application of such materials, this property is quite essential as it allows a maximum powder dispersion during the catalytic cycle and a quick isolation of the material after the reaction is complete.

3.2 Catalytic activity

The catalyst $\text{Fe}_3\text{O}_4@\text{ZnO}@\text{Au}$ was applied in the photodegradation of Rhodamine-B using white light as the irradiation source. The spectral time scan of degradation of Rhodamine-B using $\text{Fe}_3\text{O}_4@\text{ZnO}@\text{Au}$ as catalyst is shown in Fig. 7. For the purpose of comparison the catalyst

adsorption (no irradiation) and the photolysis (no catalyst present) curves are also shown (Fig. 7a, b). The photolysis test shows that no appreciable degradation occurs after 8 h of continuous light irradiation in the absence of the catalyst. Adsorption experiments were also carried out to assess the adsorption-desorption equilibrium. As it can be seen from Fig. 7b, the dye removal percentage after 30 min was considerably slow (<15 %), under the conditions studied. Figure 7c demonstrates the photodegradation activity of the synthesized $\text{Fe}_3\text{O}_4@\text{ZnO}@\text{Au}$ as a function of time (1–5 h). The results were obtained spectrophotometrically after the magnetic separation at the respective reaction time. Seventy five percent of the dye content was efficiently degraded after

1 h, and after 8 h the solution becomes complete clear and its concentration is below the detection limit range of the technique (<0.01 ppm).

The possibility of reusability of the new catalyst in the degradation of Rhodamine-B has also been explored using the same experimental conditions described in section 2.3. In this step, a single portion of the composite was used in different cycles with no prior drying, washing, heat stress or any other method of cleaning. After each cycle, the catalyst was magnetically collected by placing a small Nd magnet on the reactor wall. Once the catalyst was completely isolated and confined by the applied magnetic field, the colorless liquid was removed and new sample of Rhodamine-B solution was added and submitted to the established reaction conditions so that a new cycle could be carried out. Figure 8 shows the percentage of degradation as a function of cycle number. As it can be seen a degradation higher than 85% is observed for the five initial cycles. This observation suggests that not only is the new catalyst highly efficient in the degradation of the targeted pollutant but It also has remarkable chemical and physical stability which are also properties highly sought-after by the catalyst industry. After the 6th cycle a significant drop in catalyst activity is observed but It still exhibits a degradation higher than 56% after the 12th cycle. These results are quite remarkable when compared to other reported photocatalysts under similar conditions for the degradation of Rhodamine-B solutions. The mechanism of photodegradation by ZnO@Au particles are well established [1], and the high

efficiency obtained by the new catalyst is unlikely to be linked to a different mechanistic path but rather to the high dispersion of Au nanoparticles on the mesoporous structure of the ZnO layer.

4 Conclusions

In summary, a catalytic composite for the photodegradation of Rhodamine-B with intrinsic magnetic properties was synthesized. A modified method using the thermal decomposition of urea in the presence of ZnO precursor, and magnetite nanoparticles stabilized by CTAB led to the formation of a mesoporous ZnO matrix containing Fe_3O_4^- implanted nanoparticles. The material was used as a platform for the fabrication of highly dispersed Au nanoparticles (~ 5 nm). The catalyst, $\text{Fe}_3\text{O}_4@\text{ZnO}@\text{Au}$, was efficiently applied in the photodegradation of Rhodamine-B solutions and a degradation higher than 99% was obtained. Catalyst recycling study showed that a single portion of the material could be repeatedly used up to five times without significant loss of its activity, and the catalyst was still considered active even after the 12th cycle (degradation higher than 56%). The magnetic property allowed a simple and straightforward separation after each run using a small Nd magnet. The use of urea as the pH regulator reduced the formation of non-magnetic ZnO species and a higher mass yield of the magnetic was achieved (1.5 \times) compared to the protocol using NaOH. From the exposed results, we believe that this novel strategy to fabricate $\text{Fe}_3\text{O}_4@\text{ZnO}$ more efficiently is of great interest in designing multifunctional catalytic solids, and It can be also applied as anchoring sites for the preparation of other metal nano-catalysts.

Acknowledgements The authors are grateful to Fundação de Amparo a Pesquisa do Estado de Mato Grosso (FAPEMAT) and Conselho Nacional de Desenvolvimento Científico e Tecnológico (CNPq) for financial support, and indebted to LNNano-Brazil, LME-DEMA-UFSCAR and LMC-UnB for XPS, TEM and BET analyses, respectively.

Compliance with ethical standards

Conflict of interest The authors declare that they have no conflict of interest.

References

1. Fageria P, Gangopadhyay S, Pande S (2014) Rsc Adv 4 (48):24962–24972
2. Nagaraja R, Kottam N, Girija CR, Nagabhushana BM (2012) Powder Technol 215:91–97
3. Singh S, Barick KC, Bahadur D (2013) J Mater Chem A 1:3325–3333

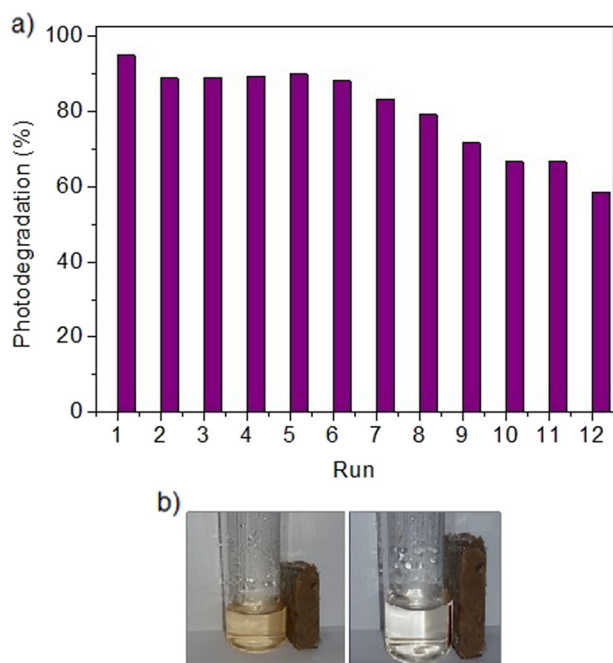


Fig. 8 a Recycling profile of $\text{Fe}_3\text{O}_4@\text{ZnO}@\text{Au}$ and b Scheme of magnetic catalyst isolation after degradation completion

4. Zhang K, Zhou W, Zhang X, Qu Y, Wang L, Hu W, Tian G (2016) *RSC Adv* 6:50506–50512
5. Chamjangali MA, Boroumand S (2013) *J Braz Chem Soc* 24 (8):1329–1338
6. Hernández S, Hidalgo D, Sacco A, Chiodoni A, Lamberti A, Cauda V, Saracco G (2015) *Phys Chem Chem Phys* 17 (12):7775–7786
7. Height MJ, Pratsinis SE, Mekasuwandumrong O, Praserthdam P (2006) *Appl Catal B-Environ* 3:305–312
8. Alshammari A, Bagabas A, Assulami M (2014) Photodegradation of rhodamine B over semiconductor supported gold nanoparticles: The effect of semiconductor support identity. *Arab J Chem*. <https://doi.org/10.1016/j.arabjc.2014.11.013>
9. Hu X, Xu Q, Ge C, Su N, Zhang J, Huang H, Cheng J (2016) *Nanotechnology* 28(4):045604
10. Collard X, El Hajj M, Su BL, Aprile C (2014) *Micro Mesopor Mat* 184:90–96
11. Wang F, Liang L, Shi L, Liu M, Sun J (2014) *Dalton T* 43:16441–16449
12. Yang L, Wu H, Jia J, Ma B, Li J (2017) *Micro Mesopor Mat* 253:151–159
13. Jacinto MJ, Kiyohara PK, Masunaga SH, Jardim RF, Rossi LM (2008) *Appl Catal A-Gen* 338(1):52–57
14. Nguyen VC, Nguyen NLG, Pho QH (2015) *ADV Nat Sci-Nanosc* 6(3):035001
15. Park J, An K, Hwang Y, Park JG, Noh HJ, Kim JY, Park JH, Hwang NM, Hyeon T (2004) *Nat Mater* 3:891–895
16. Kandula S, Jeevanandam P (2015) *RSC Adv* 5(7):5295–5306
17. Farrokhi M, Hosseini SC, Yang JK, Shirzad-Siboni M (2014) *Water Air Soil Pollut* 225(9):2113
18. Teng Z, Li J, Yan F, Zhao R, Yang W (2009) *J Mater Chem* 19:1811–1815
19. Worawong A, Jutarosaga T, Onreabroy W (2014) *Adv Mat Res* 979:208–211
20. Devaraj N K, Ong B H (2011) In *AIP Conference Proceedings* 1328(1):288–290
21. Lu J, Wang H, Peng D, Chen T, Dong S, Chang Y (2016) *Phys E* 78:41–48
22. Peng C, Liu Y (2013) *Appl Phys A* 111:1151–1157
23. Yamashita T, Hayes P (2008) *Appl Surf Sci* 254:2441–2449
24. Hosseini-Sarvari M, Khanivar A, Moeini F (2015) *J Mater Sci* 50 (8):3065–3074
25. Olteanu NL, Rogozea EA, Popescu SA, Petcu AR, Lazăr CA, Meghea A, Mihaly M (2016) *J Mol Catal A-Chem* 414:148–159
26. Pauporte T, Rathouský J (2007) *J Phys Chem C* 111:7639–7644